



Original Article

# A Thermal Cyclers Based on Solid-State Active Heat Pump and PID Control Algorithm Toward Biomedical Applications

Loc Pham Xuan\*, Tung Bui Thanh, Trinh Chu Duc

*VNU University of Engineering and Technology, 144 Xuan Thuy, Cau Giay, Hanoi, Vietnam*

Received 30 August 2021

Revised 22 December 2021; Accepted 09 February 2022

**Abstract:** The demand for a compact, easy-to-use, and precise thermal cyclers is always extremely high in biomedical field due to the decisive role of temperature in determining the accuracy of many biomedical applications. In this study, a new design of thermal cyclers is proposed to improve the ease of manipulation as well as production process while maintaining the required accuracy of temperature handling. Specifically, a semiconductor component called Peltier is utilized as the main heat generation source in this work, which offers an operation range of 15-80 °C. As Peltier has already been mass produced in the market and gained its popularity by appearing in many home appliances, the production cost and time could be minimized. Additionally, by applying the Proportional-Integral-Derivative (PID) control algorithm, the accuracy of the proposed system could be maintained (maximum variation within 1 °C in case of Isothermal Amplification and 2 °C in case of Temperature Cycling Amplification) as compared with other thermal cyclers with sophisticated heating technology. The thermal cyclers proposed in this work is expected to be further developed to be integrated into the microfluidic chip for rapid virus detection applications.

**Keywords:** Thermal cyclers, PID, Peltier heater, Isothermal Amplification, Temperature Cycling Amplification.

## 1. Introduction

Precise thermal control has long been considered a significant issue in a variety of areas such as physical, chemical, and biomedical field. A study by Reverberi found that

temperature acts as one of the most crucial factors affecting the antigen-antibody reaction (one of the most important types of reaction in biomedical field), along with pH, Ionic strength and Enzyme treatment [1]. Another study showed that a typical cell could be active, viable

\* Corresponding author.

*E-mail address:* [xuanloc97ars@vnu.edu.vn](mailto:xuanloc97ars@vnu.edu.vn)

<https://doi.org/10.25073/2588-1086/vnucsce.298>

with normal metabolism at exact 37 °C while at other temperature range, 8 °C for instant, the cells began to lose their attachment properties and finally their viability [2]. Therefore, in order to satisfy the required thermal conditions, heaters are often utilized to accurately provide the necessary amount of heat according to each application.

Along with the significant advancements of the microfabrication technology, heaters could therefore be produced at relatively small scale and integrated in many biomedical devices. Those mini heaters bring in numerous benefits such as low cost, low reagent consumption, compact in size and low power consumption. The applications of mini heaters, or mini thermal cyclers in other words, could mostly be seen in temperature-dependent biomedical devices, specifically nucleic acids (NA) amplification devices. Depending on specific operating procedures, NA amplification could be divided into 2 types: Temperature Cycling and Isothermal Amplification. Polymerase chain reaction (PCR) [3-5] is probably the most common technique used for NA Temperature Cycling Amplification. The method requires a typical thermal cycle to copy the target DNA/RNA of the virus until the number of the target DNA is sufficient for disease diagnosis. At first, the denaturation of a double-stranded DNA into two single-stranded DNA requires the range of temperature from 90-95 °C. After that, the annealing process of the target sequence of specific primers to the single stranded DNA takes place at 50-65 °C. Finally, the DNA extension process for duplicating two identical DNA molecules happens at 70-75 °C. The repetition of the above process results in detectable copies of the target DNA. Isothermal Amplification, on the other hand, prioritizes the stable supply of heat at a particular set point. Loop-mediated Isothermal Amplification (LAMP) [6-8], for example, is one of the most promising methods for DNA amplification. The process of LAMP includes initial step, cycling amplification step and elongation step, which are all conducted at a constant thermal condition

(about 60-65 °C). In addition, other popular Isothermal Amplification technique includes NASBA [9], which operates at constant temperature of approximately 41 °C, and HDA [10], which requires the temperature in range 45-65 °C for normal working condition.

In the past, several attempts have been made to design heaters for NA amplification applications. Hsieh et al proposed a two-dimensional, self-compensated microthermal cyler design for RT PCR, which uses array-type structure with self-compensation for better thermal uniformity [11]. In addition, other popular conventional designs for heater include block-type heaters [12], which provides high heating power due to its low electrical resistance, and serpentine-type heaters [13], which improves the edge thermal uniformity as compared with block-type heaters. However, all of the above designs require state-of-the-art equipment, expensive materials (platinum and gold), and sophisticated microfabrication technique. Consequently, a completed product would have relatively expensive cost of fabrication and time-consuming, which makes it difficult for mass-production and integration in large scale in biomedical devices.

This study proposes a novel thermal cyler, which is based on a solid-state active heat pump and controlled by PID algorithm. This approach helps to minimize the production cost and time, and therefore improve the possibility of mass production of biomedical devices that has mini heater integrated inside. The proposed thermal cyler's performance in this work will then be verified with both Temperature Cycling Amplification and Isothermal Amplification applications.

## 2. Materials and Methods

### 2.1. Overview of the System

Fig. 1a demonstrates the typical structure of a rapid virus detecting biomedical device, which includes 4 main chambers connected with each

other by fluidic channels. Technically, the sample is firstly injected into the system by an inlet. Then, it will be heated up in the heating chamber using Isothermal Amplification technique to accelerate the mixing efficiency of the sample with necessary elements. After that, the mixture goes through the Filtering Chamber [14, 15], where target substance is extracted from the mixture and then detected in the Detecting Chamber [16, 17] in later phase. The final step in the system is to collect result in the Collecting Chamber. Similar concepts have also been used in detecting the infamous COVID-19 virus [18, 19].

Fig. 1b shows the detailed structure of the proposed thermal cycler, which takes a major role in the first phase of the overall fluidic system. Basically, the heater consists of 2 main parts: the thermal cycling part and the electronic control circuit part.

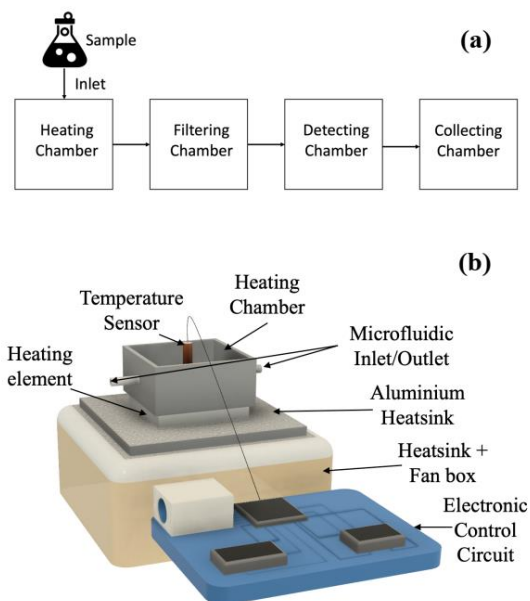


Figure 1. Overview of the system (a) Structure of a rapid virus detection flow using Isothermal Amplification technique (b) Detailed structure of the proposed thermal cycler.

Fig. 1b shows the detailed structure of the proposed thermal cycler, which takes a major role in the first phase of the overall fluidic

system. Basically, the heater consists of 2 main parts: the thermal cycling part and the electronic control circuit part.

The completed structure of the thermal cycling part in this work comprises of four elements: heating chamber, heating element, aluminum heatsink and a combination of fan and heatsink box. Those elements will be put on top of each other in the same order as listed above. The aluminum heatsink and the heatsink box with integrated fan contribute to the heat regulation process, which protects the heat generation source from being damaged due to being overheated. The heating element will be positioned on top of the heatsink by thermal adhesive to increase the contact area between the two surfaces. Finally, the heating chamber designed by a 3D software will then be put on top of the heating component. In addition, there are also inlet fluidic channels to inject the target bio-elements into the chamber for heating and outlet channels to accumulate the results after the reaction finishes.

The behavior of the heat generating part depends on the electronic control circuit, which is also illustrated in the overview figure above. Technically, the control circuit will be responsible for adjusting the heating element so as to keep the temperature inside the heating chamber as close to the user-defined setpoint as possible.

The design and fabrication of the thermal cycling part and the electronic control system will be discussed in more details in the following sections.

## 2.2. Design and Fabrication of the Thermal Cycler

In this work, a semiconductor component called Peltier is utilized as the main heat generation source for the whole system.

The component consists of 2 semiconductor blocks as shown in Fig. 2a: N-type block (electrons are the majority charge carrier) and P-type block (holes are the majority charge carrier). These 2 blocks will then be connected in series. The Peltier heater's working principle

is based on the Thermoelectric effect [20]. That is, when electric current flows through a junction between two conductors, it has the possibility to add or remove heat at that junction. In Fig. 2a, when electric current is applied to the component, the majority charge carriers of both blocks (electrons in N-type and holes in P-type) will move from the downside to the upside. Each charge carrier will carry a certain amount of heat while moving and therefore, acts as a unit of heat transfer. Eventually, when the applied current is high enough, which means more and more charge carriers will participate in the heat transfer process when moving from the downside to the upside, the Peltier component will form two states, hot junction (upside) and cold junction (downside). As the flow of the majority charge carriers decides the flow of heat transfer, the Peltier component in this study could be used both as a heater and a cooler device just by reversing the applied electric current.

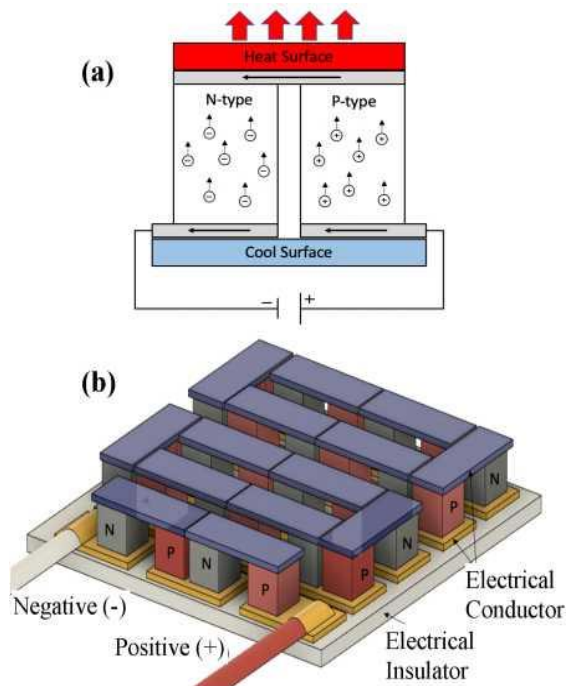


Figure 2. Working principle of Peltier heater (a) Thermoelectric effect [20], (b) Structure of a Peltier heater.

Fig. 2b depicts the actual structure of a Peltier heater. In order to increase the heating productivity, many heat transfer units (the structure of one unit is shown in Fig. 2a) are connected in series to magnify the Thermoelectric effect [20]. The substrate of the device will be coated with a layer of electrical insulator, normally ceramic.

The heating element (Peltier heater) is already available in the market and could be bought to reduce the overall fabrication time. There is a wide range of size available for the Peltier component regarding heating power. In this study, the chosen model is TES1-4903 Peltier, which has the size of 20x20 mm for substrate and 4 mm height. The maximum heating power of the device is 20 W, maximum voltage and current is 6 V – 3 A. In addition, actual experiment showed that the temperature range is from 15~80 °C, given the environment temperature is 32 °C.

In addition, the design of heating chamber used for this work will be sketched 3D by the Autodesk Fusion 360 software. The size of the chamber will be 20x20 mm for the substrate and 10 mm height. After the sketch is completed, it will be exported to STL file and finally be printed using Stratasys Object500 Connex3 3D printer. The Stratasys printer offers extremely high printing resolution, therefore, the substrate of the chamber could be fabricated as thin as 0.01 mm to maximize the heat transfer from the Peltier surface to the solution inside the chamber. The material chosen for this work is a mixture of RGD525, TangoBlack+ and VeroWhite.

### 2.3. Design of the Electronic Control System for the Thermal Cycler

Fig. 3 depicts a schematic diagram of the thermal cycling control system, which reveals the design for implementation of both hardware and software.

Regarding the hardware implementation, in the electronic control circuit block, the

microcontroller is connected to I/O interface modules such as keypad module for receiving data from users and LCD module for displaying necessary data of the system. In addition, the controlling circuit also includes drivers for each part of the thermal cyler such as driver for the heatsink system, driver for Peltier heater and circuit for reading temperature data from thermistor. The system will be powered from a DC power source, which is able to provide up to 15 V and 10 A.

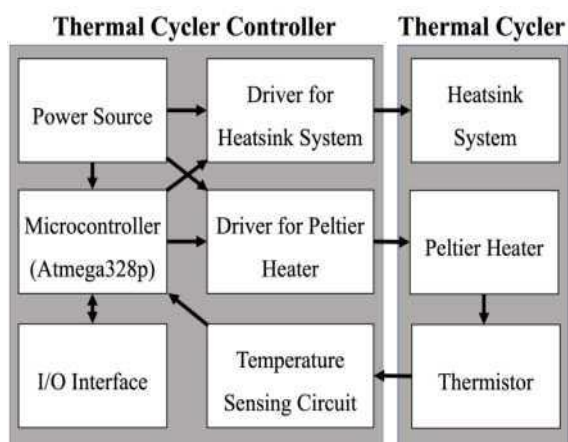


Figure 3. System Architecture.

Fig. 3 also reveals the software implementation of the system based on directional arrows. Specifically, the proposed thermal cyler operates based on the PID (Proportional-Integral-Derivative) control algorithm to optimize the performance. Technically, PID is a control algorithm that receives the feedback data, compares with a predefined setpoint and outputs an appropriate value for actuator based on the difference between set point and the feedback data. The directional arrows in the diagram form a PID control loop, which consists of microcontroller, driver for Peltier heater, Peltier heater, thermistor and temperature reading circuit. The accuracy of PID depends heavily on the appropriate combination of parameters for proportional ( $K_p$ ), integral ( $K_i$ ) and derivative ( $K_d$ ).

## 2.4. Experimental Setup

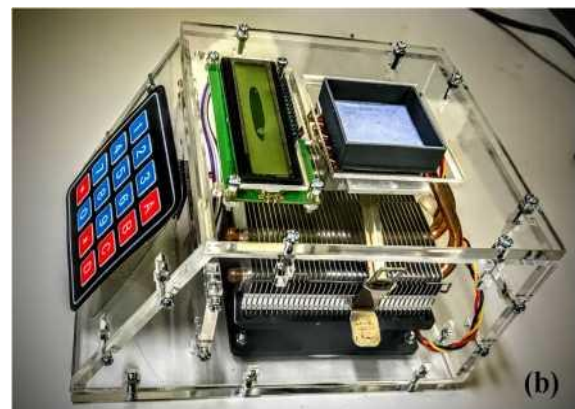
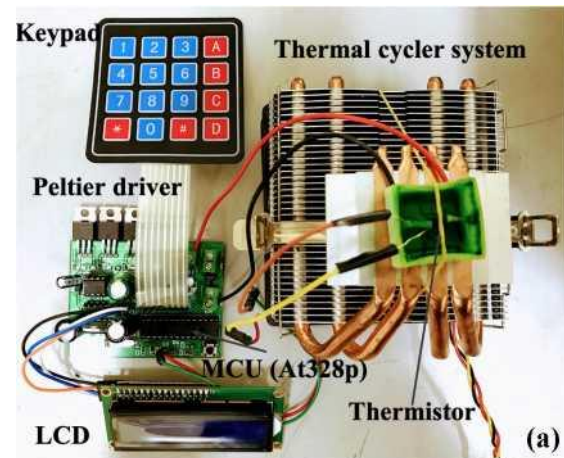


Figure 4. System Implementation.  
(a) System before packaging;  
(b) System after packaging.

Fig. 4 shows the actual implementation of the system based on the proposed architecture in Fig. 3. Specifically, the microcontroller Atmega328p from Atmel Corporation is utilized. Atmega328p belongs to the AVR family, which is famous for its compact size, high processing power, low power consumption and reasonable price. Besides, the controller circuit board also integrates the Peltier driver function, which consists of Field-Effect-Transistors (FETs) and driver ICs to form a H-bridge circuit to allow the actuator function in both directions and PWM circuit for generating desired voltages. NTC-

MF52AT 10K 3950 1% temperature sensor is connected to the MCU in the controller board to get the feedback data (current temperature inside the heating chamber). The system is also equipped with 4x4 keypad and LCD for interfacing with users (receiving and displaying necessary data). In addition, a 15 V – 10 A DC power source provides power for the whole system and a digital oscilloscope for debugging purposes.

In this work, three experiments will be conducted to verify the performance of the proposed thermal cyclers. Experiment 1 tests the response of the system in open-loop condition (no feedback from the thermistor). Experiment 2 and 3 evaluate the performance of the system in close-loop configuration by applying in Isothermal Amplification and Temperature Cycling Amplification.

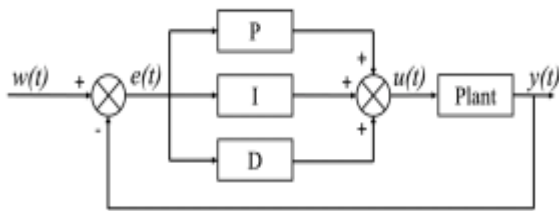


Figure 5. PID system representation in time domain

2.5. The Determination of Kp, Ki, Kd Factors

In PID controller, Kp depends on the present error, Ki depends on the accumulation of past errors, Kd represents the prediction of the future errors [21, 22].

The overall error in PID is stated as:

$$U(t) = K_p e(t) + K_i \int e(t)dt + K_d \frac{de(t)}{dt} \quad (1)$$

$$e(t) = w(t) - y(t) \quad (2)$$

where w(t) is the setpoint, e(t) is the difference between current temperature and the setpoint, U(t) is the control signal from the PID algorithm, which is then used in the “Plant” block. “Plant” represents the practical heating system, which consists of the thermistor, heating chamber, Peltier heater and so on. The control signal U(t)

is used to generate appropriate heat from the Peltier heater to the heating chamber, the temperature inside the chamber is read by the thermistor, which is represented by y(t).

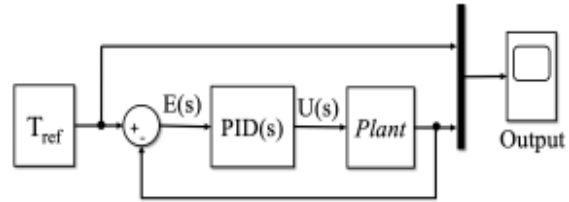


Figure 6. PID system representation in frequency domain.

The determination of factors Kp, Ki, Kd in this study is conducted by 2 methods: experiment-based and simulation-based method. The experiment-based method determines Kp, Ki, Kd by continuously adjusting the current parameters according to the actual performance of the system. The parameter adjustment is based on the rules in the table below:

Table 1. PID Parameter adjustment effects [21]

Response	Rise time	Overshoot	Settling Time	Steadystate error
Kp	Decrease	Increase	Slight decrease	Decrease
Ki	Slight decrease	Increase	Increase	Significant decrease
Kd	Slight decrease	Decrease	Decrease	Little change

On the other hand, the simulation-based method determines Kp, Ki, Kd by simulation using MATLAB. Firstly, the system representation will be transformed into the frequency domain using Laplace transformation. After that, a MATLAB function, namely Parameter Tuning, will be utilized to determine the optimal combinations of Kp, Ki, Kd, which results in the best performance for the system.

$$U(s) = K_p E(s) + K_i \frac{E(s)}{s} + K_d E(s)s \quad (3)$$

$$E(s) = T_{ref} - Output \quad (4)$$

where  $T_{ref}$  = setpoint,  $E(s)$  = error signal,  $U(s)$  = control signal,  $K_p$  = proportional gain,  $K_i$  = integral gain,  $K_d$  = derivative gain.

The parameters  $K_p$ ,  $K_i$ ,  $K_d$  in experiments conducted in the following section will be obtained by combining the above-mentioned 2 methods. Firstly, the necessary variables and parameters will be provided into the MATLAB model in Fig. 6. The system model for "Plant" block will be inferred from practical experiments. Then, applying the function offered by MATLAB, we could determine the optimum combination of  $K_p$ ,  $K_i$ ,  $K_d$  by manually tuning those parameters using the integrated Parameter Tuning function in MATLAB. At the moment, the theory-based optimum combination of  $K_p$ ,  $K_i$ ,  $K_d$  will be applied into the proposed system. However, when being applied into practical system, it will be affected heavily by random noise according to specific environment condition. The mismatch between simulation and experiments is caused by the mismatch between Gauss noise in simulation and random noise in experiments. Thus, based on specific noise from environment, those parameters will be adjusted continually based on Table. 1 until the system reaches its best performance.

### 3. Results and Discussion

#### 3.1. Experiment with Open-loop Control

Open-loop control is the simplest form of control algorithm with no feedback data. The relation between duty cycle and temperature is shown in Fig. 7. In this experiment, each duty cycle value is kept for 3 minutes, which is considered sufficient for the system to reach the thermal equilibrium state, given the change occurs after that interval is neglectable. Based on the obtained graph, a certain temperature set point could be reached just by adjusting the duty cycle to an appropriate value so that the system approaches the thermal equilibrium condition. For example, setting the duty cycle value to 9 and wait until the system reach the thermal equilibrium state will result in the final

temperature of 37 °C. Similarly, the thermal equilibrium temperature of 45 °C could be reached by setting the duty cycle value to 19, etc,...

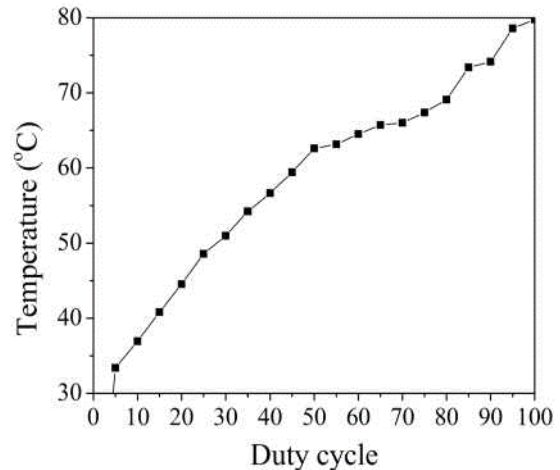


Figure 7. Duty cycle and temperature graph (in thermal equilibrium condition) with open-loop control.

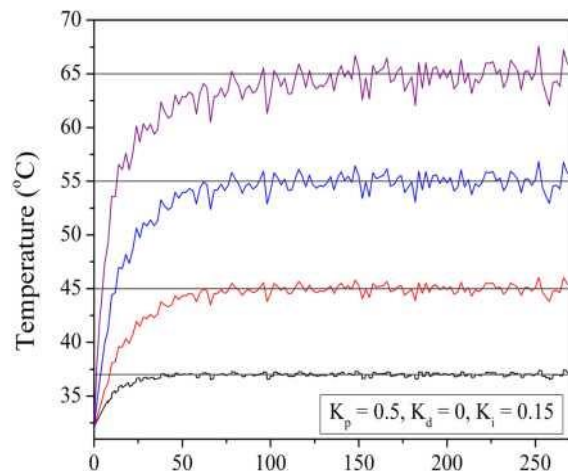


Figure 8. System performance in simulation.

The biggest advantage of this kind of control algorithm is simple implementation. However, the simplicity in implementation is traded off expensively by a relatively poor performance. Firstly, since the system has no feedback data from the heating chamber, the microcontroller unit could not have any response to adapt to any

possible change in the environment, which might affect the temperature at the thermal equilibrium state. Therefore, the vulnerability to changes in the environment will consequently result in biased, inaccurate, and undesired output temperature. Secondly, since each set point is equivalent to a duty cycle value in Fig. 7, the power outputting to Peltier heater is fixed from the beginning until the thermal equilibrium state. As a result, it takes significant amount of time to reach the desired temperature, at least, as compared with applying the proportional factor  $K_p$  of PID algorithm.

The characteristics of the system will be defined from Fig. 7. The obtained characteristics are then approximated by machine learning to infer system model for "Plant" block. The system performance in simulation is shown as in Fig. 8. Specifically, with the combination of  $K_p = 0.5$ ,  $K_d = 0$ ,  $K_i = 0.15$ , the system could reach the near perfect behavior with little overshoot (both initial and repetitive overshoot) and steady-state error. According to simulation, the system suffers from little overshoot, therefore it is unnecessary to use the derivative factor. In addition, Gaussian noise is also added to the system and the noise is magnified gradually as the temperature increases. The added Gaussian noise results in a maximum variation of  $\pm 0.4$  °C,  $\pm 1$  °C,  $\pm 1.9$  °C and  $\pm 3$  °C in case of 37 °C, 45 °C, 55 °C and 65 °C respectively.

### 3.2. Experiment with Close-loop Control

#### 3.2.1. Isothermal Amplification Applications

In close-loop control experiment with Isothermal Amplification application, four typical setpoints are chosen to evaluate the performance of the proposed thermal cyclers: 37 °C, 45 °C, 55 °C and 65 °C. 37 °C is the ideal temperature for normal cells to remain active and viable. Meanwhile, 45, 55, and 65 °C are popular setpoints in the operation range of Isothermal Amplification methods such as LAMP (60-65 °C), NASBA (41 °C), HDA (45-65 °C). The system's operation is also verified by 2 modes of close-loop control, that is ON/OFF control and PID control.

Fig. 9 shows detailed results regarding the comparison between ON/OFF control and PID control algorithm in four different set points. ON/OFF control is the simplest form of close loop control algorithm. Based on the received feedback data from the thermistor, the maximum power is outputted to the Peltier heater while the current temperature is less than the pre-defined set point. On the other hand, in case the current temperature surpasses the pre-defined set point, the microcontroller will stop the Peltier heater to cool down the system until its temperature equals to the desired set point. The close-loop in ON/OFF control mode ensures that the system has the capability to adapt to changes in the environment and significantly speed up the process as compared with open-loop control. However, this mode still has major drawbacks as can be seen in Fig. 9. In case the setpoint is 37 °C (Fig. 9a), the system consistently suffers from a relatively big overshoot of 2.5-3 °C. The overshoot then gradually decreases if the predefined set point increases, which is 2-2.5 °C of overshoot in case of 45 °C (Fig. 9b) and 1-1.5 °C (Fig. 9c) overshoot in case of 55 °C. If the desired temperature is set to 65 °C, the overshoot phenomenon disappears, instead, the system consistently fluctuates at approximately 0.1-2 °C below the setpoint level. The reason is that the ON/OFF control could not respond smartly enough to cope with the extremely high speed of heat loss at this high temperature level.

The experiment with PID control mode will be conducted with different combinations of P, I, D factors to show the step-by-step improvement of PID as compared with ON/OFF control. As can be seen from the graph in Fig. 9, PID algorithm only suffers from overshoot at the very first cycle and successfully eliminates the consistent overshoots appearing in every cycle, which is a major improvement as compared with ON/OFF control. The influence of proportional factor  $K_p$  is shown clearly in the characteristic of the red dot line. In case the set point is low (37 °C and 45 °C), the system shares relatively similar behavior, which is an overshoot of 2.5-3 °C at the beginning and gradually becomes

stable in the next sequences of cycle. However, when the system is set to be in high temperature set point (55 °C and 65 °C), it fails to adequately compensate heat to deal with the rapid heat loss caused by the environment. As a result, the temperature inside the chamber slightly fluctuates below the setpoint at approximately 1 °C in case of 55 °C and 2.5 °C in case of 65 °C. Therefore, although adding proportional factor helps enhance the system performance by increasing the heating speed and eliminating the unwanted overshoot in every cycle, it still has significant steady-state error, especially in high temperature condition, and ineffective response to changes in the environment. Those drawbacks will be solved gradually with the combination of the derivative and integral factors.

In Fig. 9, the green dash-dotted line represents the system behavior in PID mode with the combination of proportional and derivative factors. By adding the derivative factor to the control algorithm, the relatively big overshoot at the initial cycle in the red dot line has been reduced significantly. Specifically, the overshoots at 37 °C now is 1.5 °C instead of 3 °C, 1 °C overshoot at the setpoint of 45 °C instead of 2.5 °C. However, at higher setpoints (55 °C and 65 °C), the green dash-dotted line shows little improvements as compared with the red dot line, both could not adapt to the rapid heat loss due to high temperature environment. The steady-state error existing in the previous cases will be fixed when adding the integral factor. With the complete combination of P, I, D factors, the system shows a significantly stable performance at all setpoints. At the setpoint of 37 °C, the KPID line nearly approaches the reference line with the maximum bias of -0.4 °C only. In case of 45 °C, the KPID line slightly fluctuates above the reference line with the maximum bias of +0.5 °C. The stable performance still exists even in the high temperature environment (55 °C and 65 °C). The fluctuation is  $\pm 0.7$  °C and +1 °C respectively. The only drawback is a small increase in overshoot as compared with the green dash-dotted line of P, D combination. The practical

results are comparable to simulation in ideal temperature level and more stable in high temperature environment.

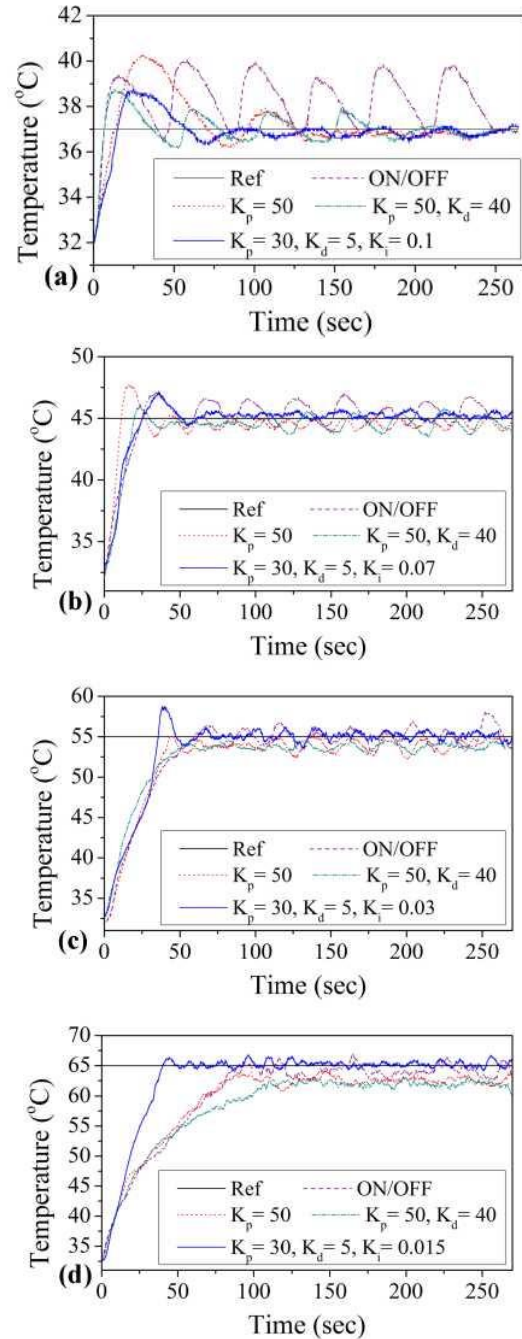


Figure 9. Comparison of ON/OFF control and PID control (P, PD, PID) with different setpoints. (a) Comparison at 37 °C, (b) Comparison at 45 °C, (c) Comparison at 55 °C (d) Comparison at 65 °C.

Regarding response time, with a complete combination of P, I, D, the system needs 15 seconds to heat up from 32 °C to 37 °C and roughly 90 seconds to reach the stable state. In case the setpoint is 45 °C, it takes 30 seconds to reach the target and 80 seconds to stabilize. In case of 55 °C and 65 °C, response time is approximately 40 seconds and stabilization time is 70 seconds and 60 seconds respectively. All experiments were conducted in the room temperature of 32 °C. The results above suggests that in the proposed heater, the bigger the setpoint, the longer the response time and the shorter the stabilization time.

According to the obtained results above (maximum variation is only 1 °C and reasonable response time), the proposed heater could be well-applied into most Isothermal applications such as LAMP (60-65 °C) [6], HDA (45-65 °C) [10].

### 3.2.2. Temperature Cycling Amplification Applications

Fig. 10 reveals the system behavior in the application of “Temperature Cycling Amplification” with PID control algorithm. This experiment will simulate the thermal cycling process of a PCR device with three set points: 45 °C, 55 °C and 65 °C. Basically, the performance is similar to the isothermal application. That is, the overshoot at 45 °C is approximately 1.2 °C and the fluctuation as compared with the reference line is -0.4 °C. However, the performance at 65 °C is not as expected, as the controller fails to deal with the rapid heat loss of the high temperature condition, which results in a fluctuation in range of 63-64 °C. The last stage of the thermal cycler is cooling down from 65 °C to 55 °C. At 55 °C, the system has an acceptable performance with a fluctuation of  $\pm 1$  °C.

Regarding response time, the system performance is not as good as Isothermal experiments. Specifically, in the first phase, the response time and stabilization time is comparable to Isothermal experiments, however, it takes nearly 2 minutes to heat from 45 °C to approach 65 °C. In the last phase, it needs about 15 seconds to cool down to 55 °C and 40 more seconds to be stable.

The performance of the system in Temperature Cycling Amplification is not as good as Isothermal Amplification. The reason is that each setpoint in Isothermal experiment is carefully calibrated to determine the most suitable combination of  $K_p$ ,  $K_i$ ,  $K_d$ , meanwhile, when these separated setpoints are combined to form a temperature cycle, the calibration becomes more challenging and less accurate. Despite of that, the performance of the system in Temperature Cycling Amplification (maximum variation is 2 °C) still has potential to be applied into real-life applications, which requires a cycle of temperature. For the Peltier chosen in this work, its relatively low power (only 20W) only offers an operating range of 15-80 °C, which is insufficient to be used in PCR (the most popular application of Temperature Cycling Amplification). However, a more powerful Peltier with exactly the same setting as in this work will increase the operating range and therefore, could be qualified to be used in PCR application.

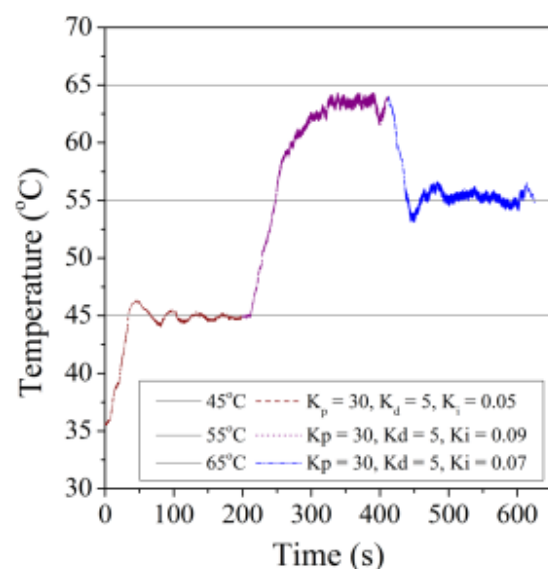


Figure 10. Temperature Cycling Amplification with PID control algorithm.

In the future, other advanced control algorithms such as fuzzy logic could be applied to the system instead of PID to further improve

the efficiency of temperature control. However, in the scope of this work, the proposed system prioritizes the simplicity, and practical experiments also prove that traditional PID control is adequately good to handle the thermal requirements in cell culture systems.

## 5. Conclusion

This study proposes a novel approach of building thermal cyler based on a solid-state active pump called Peltier. This new design method significantly reduces the fabrication time, cost and the complexity of device manipulation as compared with previous designs. While the fabrication and manipulation process are simplified, the proposed heater could still satisfy necessary requirements to be used in a wide range of biomedical applications. With the complete combination of the proportional-integral-derivative factors, in Isothermal mode, the system could operate smoothly with the error less than 0.5 °C under ideal condition (<50 °C), less than 1 °C under high temperature condition (>50 °C), and less than 2 °C in Temperature Cycling mode. Thus, the proposed heater could be potentially applied in various biomedical applications such as Isothermal Amplification (LAMP, NASBA,...) and Temperature Cycling Amplification (PCR). In the future scope, the fluidic system proposed in Fig. 1a could be minimized to fit into a small PCB and the heater could be integrated into that PCB using microfabrication technique, which serves as a foundation to complete a portable microfluidic biomedical device for rapid virus or cell detection.

## References

- [1] R. Reverberi, L. Reverberi, Factors Affecting the Antigen-antibody Reaction, *Blood Transfus*, Vol. 5, No. 4, 2007, pp. 227-240.
- [2] J. C. Encarnação, P. Barta, T. Fornstedt, K. Andersson, Impact of Assay Temperature on Antibody Binding Characteristics in Living Cells: A Case Study, *Biomed. Reports*, Vol. 7, No. 5, 2017, pp. 400-406.
- [3] K. Mullis, F. Faloona, S. Scharf, R. Saiki, G. Horn, H. Erlich, *Specific Enzymatic Amplification of DNA in Vitro: the Polymerase Chain Reaction*. 1986, *Biotechnology*, Vol. 24, 1992, pp. 17-27.
- [4] R. Higuchi et al., Simultaneous Amplification and Detection of Specific DNA Sequences, *Nature Biotechnology*, Vol. 10, 1992.
- [5] T. Pogfai, K. W. Ek, S. Mongpranet, A. Wisitsoraat, A. Tuantranont, Low Cost and Portable PCR Thermoelectric Cycle, *Int. J. Appl. Biomed. Eng.*, Vol. 1, No. 1, 2008, pp. 41-45.
- [6] T. Notomi et al., Loop-Mediated Isothermal Amplification of DNA, *Nucleic Acids Res.*, Vol. 28, No. 12, 2000, pp. E63.
- [7] J. H. Jung, B. H. Park, S. J. Oh, G. Choi, T. S. Seo, Integration of Reverse Transcriptase Loop-Mediated Isothermal Amplification with An Immunochromatographic Strip on A Centrifugal Microdevice for Influenza A Virus Identification, *Lab Chip*, Vol. 15, No. 3, 2015, pp. 718-725.
- [8] X. Fang, Y. Liu, J. Kong, X. Jiang, Loop-Mediated Isothermal Amplification Integrated on Microfluidic Chips for Point-of-Care Quantitative Detection of Pathogens, *Anal. Chem.*, Vol. 82, No. 7, 2010, pp. 3002-3006.
- [9] J. Compton, Nucleic Acid Sequence-Based Amplification, *Nature*, Vol. 350, No. 6313, 1991, pp. 91-92.
- [10] M. Vincent, Y. Xu, H. Kong, Helicase-Dependent Isothermal DNA Amplification, *EMBO Rep.*, Vol. 5, No. 8, 2004, pp. 795-800.
- [11] T. M. Hsieh, C. H. Luo, J. H. Wang, J. L. Lin, K. Y. Lien, G. Bin Lee, A Two-Dimensional, Self-Compensated, Microthermal Cyler for One-Step Reverse Transcription Polymerase Chain Reaction Applications, *Microfluid. Nanofluidics*, Vol. 6, No. 6, 2009, pp. 797-809.
- [12] C. S. Liao et al., Micromachined Polymerase Chain Reaction System for Multiple DNA Amplification of Upper Respiratory Tract Infectious Diseases, *Biosens. Bioelectron.*, Vol. 20, No. 7, 2005, pp. 1341-1348.
- [13] D. S. Yoon et al., Precise Temperature Control and Rapid Thermal Cycling in A Micromachined DNA Polymerase Chain Reaction Chip, *J. Micromechanics Microengineering*, Vol. 12, No. 6, 2022, pp. 813-823.
- [14] R. Zhou, C. Wang, Microfluidic Separation of Magnetic Particles with Soft Magnetic Microstructures, *Microfluid. Nanofluidics*, Vol. 20, No. 3, 2016, pp. 1-11.
- [15] L. Amato, Y. Gu, N. Bellini, S. M. Eaton, G. Cerullo, R. Osellame, Integrated Three-

- Dimensional Filter Separates Nanoscale from Microscale Elements in A Microfluidic Chip, *Lab Chip*, Vol. 12, No. 6, 2012, pp. 1135-1142.
- [16] L. Q. Do et al., Dielectrophoresis Microfluidic Enrichment Platform with Built-in Capacitive Sensor for Rare Tumor Cell Detection, *Biochip J.*, Vol. 12, No. 2, 2018, pp. 114-122.
- [17] Q. L. Do, T. T. Bui, T. T. H. Tran, K. Kikuchi, M. Aoyagi, T. C. Duc, Differential Capacitively Coupled Contactless Conductivity Detection (DC4D) Sensor for Detection of Object in Microfluidic Channel, 2015 IEEE SENSORS - Proc., 2015, pp. 5-8.
- [18] K. R. Sreejith et al., A Portable Device for Lamp Based Detection of Sars-Cov-2, *Micromachines*, Vol. 12, No. 10, 2021.
- [19] K. G. De Oliveira, P. F. N. Estrela, G. D. M. Mendes, C. A. Dos Santos, E. D. P. S. Lacerda, G. R. M. Duarte, Rapid Molecular Diagnostics of COVID-19 by RT-LAMP in A Centrifugal Polystyrene-toner Based Microdevice with End-point Visual Detection, *Analyst*, Vol. 146, No. 4, 2021, pp. 1178-1187.
- [20] L. Li, J. H. Jiang, Staircase Quantum Dots Configuration in Nanowires for Optimized Thermoelectric Power, *Sci. Rep.*, Vol. 6, 2016.
- [21] A. Jenkins, PID Controller Tuning Using Ziegler-Nichols Tuning Formula, 2019, pp. 1289-1296.
- [22] B. Diriba, H. Prof, W. Zhongmin, Design and Control for Differential Drive Mobile Robot, Vol. 6, No. 10, 2017, pp. 327-335.